Estrogen receptor alpha inhibits mesenchymal and amoeboidal movement of liver cancer cell via G protein subunit alpha 12

Jessica Yun[1], Mi Jeong Heo[1], Yun Seok Kim[1], Min Joo Kim[2], Aree Moon[2], and Sang Geon Kim[1]

[1]Seoul National University
[2]Duksung Women's University

November 24, 2020

Abstract

Background and Purpose Hepatocellular carcinoma (HCC) is the second most common cancer worldwide, demonstrating aggressiveness and mortality more frequently in men than in women. Despite reports regarding the inhibitory ability of estrogen receptor alpha (ERα, ESR1) in certain cancer progression, targets and the basis of underlying gender disparity in HCC worsening remain elusive. Experimental Approach Human HCC samples were used for immunoblottings and immunohistochemistry. Estradiol (E2) was treated to HCC cell lines and were evaluated by immunoblottings, polymerase chain reaction, immunofluorescence, and live imaging. Key Results Here, we report the ability of ERα to transcriptionally inhibit G protein subunit alpha 12 (Gα12). First, using human samples and public database, the expression of ERα and Gα12 in HCC was examined. Then, quantitative real-time PCR, chromatin immunoprecipitation-assay, luciferase assay, and immunoblottings confirmed the inhibitory ability of ERα on Gα12 and EMT. Additionally, we found microRNA-141 and -200a as downstream targets of the Gα12 signaling axis for cancer malignancy regulation under the control of ERα. As for in-depth mechanism, PTP4A1 was found to be directly inhibited by microRNA-141 and -200a. Gα12 and PTP4A1 promoted epithelial-mesenchymal transition, as well as mesenchymal to amoeboidal transition, antagonized by ERα modulations. Conclusion and Implications The identified targets and ESR1 levels inversely correlated in human specimens, as well as with sex-biased survival rates of HCC patients. Collectively, ERα-dependent repression of Gα12 and consequent changes in the Gα12 signaling may explain the gender disparity in HCC, providing pharmacological clues for the control of metastatic HCC.

Estrogen receptor alpha inhibits mesenchymal and amoeboidal movement of liver cancer cell via G protein subunit alpha 12

Short title: ERα inhibition of Gα12

Jessica Yun[1], Mi Jeong Heo[1], Yun Seok Kim[1], Min Joo Kim[2], Aree Moon[2], and Sang Geon Kim[3,1,*,#]

[1]*College of Pharmacy, Seoul National University, Seoul, Republic of Korea,* [2]*Duksung Innovative Drug Center, College of Pharmacy, Duksung Women's University, Seoul, Republic of Korea; and* [3]*College of Pharmacy and Integrated Research Institute for Drug Development, Dongguk University_Seoul, Goyang 10326, Kyeonggi-do, Republic of Korea*

[*]**Correspondence to:** SG Kim, Tel: +8231-961-5218; Fax: +8231-961-5206; E-mail: sgkim@dongguk.edu

[#]Lead Contact

Word Count : 4303

University fund.

Authors' Contributions

Study concept and design; acquisition of data; analysis and interpretation of data; drafting of the manuscript; statistical analysis: Jessica Yun and Mi Jeong Heo

Acquisition of data; analysis and interpretation of data; statistical analysis for liver cancer: Jessica Yun, Mi Jeong Heo, and Yun Seok Kim

Acquisition of invasion and migration data and xenograft experiment: Min Joo Kim and Aree Moon

Material and administrative support; analysis and interpretation of data: Jessica Yun, Mi Jeong Heo, and Yun Seok Kim

Study concept and design; analysis and interpretation of data; manuscript writing; critical revision of the manuscript for important intellectual content; obtained funding; administrative, technical, or material support; and study supervision: Sang Geon Kim

Conflict of Interests Statement

The authors declare no conflicts of interest.

Background and Purpose

Hepatocellular carcinoma (HCC) is the second most common cancer worldwide, demonstrating aggressiveness and mortality more frequently in men than in women. Despite reports regarding the inhibitory ability of estrogen receptor alpha (ERα, *ESR1*) in certain cancer progression, targets and the basis of underlying gender disparity in HCC worsening remain elusive.

Experimental Approach

Human HCC samples were used for immunoblottings and immunohistochemistry. Estradiol (E2) was treated to HCC cell lines and were evaluated by immunoblottings, polymerase chain reaction, immunofluorescence, and live imaging.

Key Results

Here, we report the ability of ERα to transcriptionally inhibit G protein subunit alpha 12 (Gα12). First, using human samples and public database, the expression of ERα and Gα12 in HCC was examined. Then, quantitative real-time PCR, chromatin immunoprecipitation-assay, luciferase assay, and immunoblottings confirmed the inhibitory ability of ERα on Gα12 and EMT. Additionally, we found microRNA-141 and -200a as downstream targets of the Gα12 signaling axis for cancer malignancy regulation under the control of ERα. As for in-depth mechanism, PTP4A1 was found to be directly inhibited by microRNA-141 and -200a. Gα12 and PTP4A1 promoted epithelial-mesenchymal transition, as well as mesenchymal to amoeboidal transition, antagonized by ERα modulations.

Conclusion and Implications

The identified targets and *ESR1* levels inversely correlated in human specimens, as well as with sex-biased survival rates of HCC patients. Collectively, ERα-dependent repression of Gα12 and consequent changes in the Gα12 signaling may explain the gender disparity in HCC, providing pharmacological clues for the control of metastatic HCC.

Key words : liver cancer, metastasis, estrogen receptor alpha, Gα12, PTP4A1

Introduction (516 words)

Hepatocellular carcinoma (HCC) is the fourth leading cause of death among cancers (Bray et al., 2018). Epidemiologically, HCC has revealed gender disparity, demonstrating higher morbidity and mortality in male patients (Fitzmaurice et al., 2017). The biased favoring females in HCC development and progression

suggests sex hormones (i.e., estrogens and androgens) may play distinct roles (Barreca et al., 1993). However, the role of estrogens preventing HCC progression, as well as in normal liver functions, remains elusive. In HCC, expression of estrogen receptor alpha (ERα) appears to inversely correlate with larger tumors, proliferation, migration, and invasion (Naugler et al., 2007; Yang et al., 2012; Liu et al., 2009). In addition, the repression of ERα causes tumorigenesis in HCC (Bigsby RM and Caperell-Grant A, 2011; Wu et al., 2017). Therefore, it needs to be resolved whether estrogen and ERα signaling mitigate HCC progression, and if so, the underlying basis needs to be elucidated.

Epithelial to mesenchymal transition (EMT) describes the movement of the cytoskeletal organization to allow cells to detach and disseminate by degrading the extracellular membrane (Choi and Diehl, 2009). As HCC demonstrates a poor prognosis owing to its metastatic phenotype, EMT is recognized as a key process in tumor metastasis. Thus, EMT is more frequently observed in metastatic cancer cells (Nieto, 2013; Thiery et al., 2009). Among several biomarkers observed in HCC, G protein subunit alpha 12 (Gα12), *gep* oncogene, whose gene expression product is overly expressed in metastatic HCC, is a driver gene for HCC progression, mediated by alterations in microRNAs (miRNAs) and mouse double minute 2 homolog expression (Yang et al., 2015; Heo et al., 2014).

Cancer cells adopt different motility for dissemination, presenting an obstacle for developing treatments. Mesenchymal movement forms an elongated phenotype, whereas amoeboid motility presents a round morphology (Nobes and Hall, 1995; Panková et al., 2010). Hence, the invasion/migration of cancer cells consists of not only mesenchymal but also amoeboidal movements (Sahai and Marshall, 2003). Furthermore, it has been recognized that Rho/ROCK may play a role in the amoeboid movement, which is one of the main downstream targets of the Gα12 signaling pathway (Seasholtz et al., 1999). Therefore, it is important to examine the ways cancer cells migrate and invade to prevent progression of metastatic cancers.

This study investigated whether ERα level in HCC is associated with that of Gα12 as well as the consequent changes observed in overall survival rates of the patients. In cellular models and human sample analyses, we identified the link between ERα and Gα12. Molecular studies confirmed the ERα ability to inhibit Gα12 (*GNA12*), newly revealing miR-141 and -200a as downstream targets of the Gα12 signaling axis, in conjunction with ERα expression change. Moreover, we discovered protein tyrosine phosphatase type IVA 1 (PTP4A1) as a direct target of miR-141 and -200a and the consequent changes in phosphorylated-myosin light chain (p-MLC) levels, a protein responsible for amoeboid movement downstream of Gα12 pathway. Functionally, we demonstrated the regulatory effect of Gα12 on amoeboid motility under the inhibitory control of ERα, clarifying the molecules responsible for HCC malignancy, as well as for gender disparity and prognosis in HCC patients.

Materials and Methods (1,921)

Antibodies and reagents

ICI 182,780 (I4409) and anti-β-actin (A5441) antibodies were purchased from Sigma-Aldrich (St Louis, MO, USA). Doxycycline (324385) and estrogen (3301) were obtained from Sigma-Aldrich (St Louis, MO, USA). Anti-ERα (8002), anti-Vimentin (32322), anti-ZEB1 (25388), and anti-Gα12 (515445) antibodies were provided from Santa Cruz Biotechnology (Santa Cruz, CA, USA). Antibodies directed against p-MLC (ser19) were obtained from Cell Signaling (Beverly, MA, USA) (3671). Anti-E-cadherin antibody was purchased from BD Biosciences (San Jose, CA, USA) (610181). Anti-PTP4A1 antibody was supplied from Proteintech (Chicago, IL, USA) (11508-1-AP). Antibodies obtained from Santa Cruz Biotechnology were used at a ratio of 1:1000 dilution, whereas the others were done in 1:5,000-10,000 dilution.

Cell culture

HepG2 cell (RRID: CVCL_0027) was supplied from ATCC (Manassas, VA). HEK293A and HEK293T cells were provided from American Type Culture Collection (Manassas, VA, USA). Huh7, SK-Hep1, SNU387, and SNU449 cell lines were purchased from Korean Cell Line Bank (KCLB, Seoul, Korea). All human cell lines had been authenticated using STR profiling within the last three years. All experiments were

3

performed with mycoplasma-free cells. Huh7, HepG2, HEK293A, HEK293T, SNU449, and SK-Hep1 cells were maintained in Dulbecco's modified Eagle's medium containing 10% fetal bovine serum, 50 units/mL penicillin, and 50 μg/mL streptomycin at 37°C in a humidified atmosphere containing 5% CO2. SNU387 cells were cultured in RPMI 1640 supplemented with 10% fetal bovine serum and 1% penicillin-streptomycin at 37°C in a humidified atmosphere containing 5% CO2.

Immunohistochemistry

Formalin-fixed, paraffin-embedded HCC and NT liver samples were cut using a microtome into 4 μm thickness. The tissue sections were mounted on glass slides. Antibodies of interest (ERα, Gα12, PTP4A1, p-MLC, and vimentin) were incubated overnight at room temperature with the slide-mounted method.

Human liver samples

The 59 paired samples of HCC and NT tissue were obtained from 187 patients who underwent curative surgical resection and donated samples to the Bio-Resource Center at the Asan Medical Center (Seoul, South Korea) between the years of 2006 and 2009. Tumors were classified according to the World Health Organization pathologic classification system. All patients provided informed consents, and the study protocol was approved by institutional review board of Asan Medical Center (no. 2012-0133) in accordance with the ethical guidelines of the 1975 Declaration of Helsinki.

Transient transfection

ERα and PTP4A1 expression clones were purchased from Genecopoeia (Rockville, MD). The empty plasmid, pcDNA3.1 and pCMV, was used for mock transfection. Cells were transfected with the indicated plasmid (1 μg) using Lipofectamine 2000 (Invitrogen, Carlsbad, CA) according to the manufacturer's instructions. Scrambled small interfering RNA (control siRNA), or siRNA specifically directed against ERα, Gα12, and PTP4A1 were purchased from Dharamacon (Lafayette, CO, USA). The cells were transfected with plasmid or small-interfering RNA (siRNA) using Lipofectamine 2000 transfection reagent (Invitrogen, Carlsbad, CA) for 72 h.

Establishment of stable cell lines

The virus productions were carried out using HEK293T cells. Briefly, cells were transfected with lentiviral DNA constructs combined with the lentiviral packaging plasmids pMD2G, pMDLg and pRSV-Rev and FuGENE ® HD Reagent (Roche, Indianapolis, IN). The viral supernatants were harvested 24 and 48 hours post-transfection and used for infections. Then 300 μL of virus containing culture medium was added to the cells. To establish stable cell lines, SK-Hep1 cells were infected with rtTA3 lentivirus and selected with hygromycin. The selected cells were infected with tetracycline (Tet)- On ERα lentiviruses and were selected with puromycin. A Tet On lentiviral plasmid containing the ERα sequence was synthesized by Cosmogenetech (Seoul, Korea). The plasmid TetO-FUW-pgk-puro from Emily Dykhuizen (Addgene plasmid # 85747), pLenti CMV rtTA3 Hygro (w785-1) from Eric Campeau (Addgene plasmid # 26730), pMDLg/pRRE from Didier Trono (Addgene plasmid # 12251), pRSV-Rev from Didier Trono (Addgene plasmid # 12253), and pMD2.G from Didier Trono (Addgene plasmid # 12259) were provided by Addgene (http://www.addgene.org). For conditional ERα overexpression, doxycycline (Dox) 2 μg/ml was treated in SK-Hep1 cells.

Bioinformatics analyses

RNA-seq data from Gene Expression Omnibus (GEO, https://www.ncbi.nlm.nih.gov/geo/) (GSE40367, GSE94016) was subjected to Kyoto Encyclopedia of Genes and Genomes (KEGG) enriched pathway analysis (pathway in cancer) using the DAVID 6.7 (http://david.avcc.ncifcrf.gov/ref) online bioinformatics tool. Gene interaction analysis between the clustered genes was achieved according to STRING v9.1 database (http://string-db.org). The potential targets of miRNAs of interest were extracted from TargetScan database (http://targetscan.org). Gene ontology-based functional groups of miRNA targets were searched using the DAVID 6.7 (http://david.avcc.ncifcrf.gov/ref) online bioinformatics tool.

4

Transcriptome data GEO (https://www.ncbi.nlm.nih.gov/geo/) (GSE9843, 40367, 76427) was analyzed using gene set enrichment analysis (GSEA) 3.0 software. 'Biological process of gene ontology (GO)' from Molecular Signature Database (MSigDB, http://software.broadinstitute.org/gsea/msigdb) v6.2 was employed. False discovery rate (FDR) was used for statistical significance assessment of normalized enrichment score (NES). The criterion for statistical significance was set at FDR<0.25. Heat map represents the respective leading-edge subsets of the most upregulated genes.

Luciferase activity

The plasmids of Luc-*GNA12* -3'untranslated region (UTR) and Luc-*PTP4A1* -3'UTR were specifically synthesized (GeneCopoeia, Rockville, MD), and were used in luciferase reporter assays. The plasmid contains firefly luciferase gene fused to the 3'UTR of human Gα12 (or PTP4A1), and Renilla luciferase that functions as a tracking gene. Luciferase activity assays were done according to manufacturer protocols. Briefly, HEK293A cells were seeded in 6-well plates, and co-transfected with ERα and wild type (WT) vectors, and Gα12 3' UTR WT reporter. Similarly, SNU449 or HepG2 cells were seeded in 6-well plates, and co-transfected with miR-141 and -200a mimic (or antisense oligonucleotide (ASO)), and PTP4A1 3'UTR WT reporter. The cells were harvested following transfection for 48 h. Firefly and Renilla luciferase activities were measured sequentially with the dual luciferase assay kit (GeneCopoeia). The activities were normalized with Renilla luciferase activities and expressed in relative luciferase activity units. The cells were transfected with plasmid using Lipofectamine 2000 transfection reagent (Invitrogen, Carlsbad, CA) for 48 h.

Chromatin immunoprecipitation (ChIP) assays

ChIP assays were carried out using the EZ ChIP Kit (Millipore, Billerica, MA, USA) according to the manufacturer's protocol. SK-Hep1 cells were treated with Dox and E2 for 24 h each, and then formaldehyde was added to the cells to a final concentration of 1% for cross-linking of chromatin. The ChIP assay was performed according to the ChIP assay kit protocol (Upstate Biotechnology, Lake Placid, NY). PCR was done using the primers flanking the putative ERα binding sites located in the promoter region of human *GNA12* gene. IgG immunoprecipitation represents negative control. The primer sequences used for the qPCR analysis were as follows:

Site #1

Forward: 5'- TCAAGTGATCCTCCCACCTC -3'

Reverse: 5'- TGGCTTCATTTCTGGGTTCT -3'

Site #2

Forward: 5'- CAAGGTTGTCAGGGAGTTGG -3'

Reverse: 5'- GGCACGGTGACTCACAACTA -3'

Immunocytochemistry

SK-Hep1 cells treated with Dox and E2 (24 h) were grown on a coverslip and were fixed in a 4% paraformaldehyde solution followed by permeabilization with 0.3% Triton X-100 (Sigma Aldrich). After washing with PBS, the cell samples were immunostained with antibodies directed against ERα and Gα12. Alexa Fluor 488 goat anti-mouse IgG (Invitrogen) and Alexa Fluor 594 goat anti-rabbit IgG (Invitrogen) were used as secondary antibody. After incubation, 1/10 diluted drop of Hoechst was treated for another 15 minutes. Then, the samples were cover-slipped with mounting media, and were examined using laser-scanning confocal microscopes (Leica TCS NT and Leica TCS8, Leica Microsystems, Wetzlar, Germany).

RNA isolation and quantitative reverse transcription-polymerase chain reaction (qPT-PCR) assays Total RNAs were extracted with the Trizol (Invitrogen, Carlsbad, CA, USA). qRT-PCR assays for messenger RNAs (mRNAs) were performed using StepOne real-time PCR instrument (Thermo Fisher Scientific) and SYBR Premix Ex TaqII kit (Takara Bio, Shiga, Japan), whereas those for miRNAs were carried out using

miScript SYBR Green PCR Kit (Qiagen) according to the manufacturer's instruction. The primer sequences were as follows:

β-aςτιν , 5'- ACCCACACTGTGCCCATCTAC -3' and 5'- TCGGTGAGGATCTTCATGAGGTA -3';

18s RNA , 5'- GTAACCCGTTGAACCCCATT -3' and 5'- CCATCCAATCGGTAGTAGCG -3';

GNA12 , 5'- CTCAAGGGCTCAAGGGTTCTT -3' and 5'- CAGGAACATCCCATGCTTCTC -3';

ESR1 , 5'- GAGTAACAAAGGCATGGAGCA -3' and '5- ATGAAGTAGAGCCCGCAGTG -3';

PRL-1 , 5'- ACCAATGCGACCTTAAACAAA -3' and 5'- AATCTGGTTGGATGGTGGTG-3'; and

VIM , 5'- AAGGTCAAGACGTGCCAGAG -3' and 5'- TTCCAGTTCTGCACGGTCTC -3'

qRT-PCR assays for miRNAs

cDNA was generated from equal amounts of total RNA per sample (1 μg) using the miScript Reverse Transcription kit (Qiagen GmbH, Hilden, Germany). The reaction mixture containing reverse transcription product, 2×QuantiTect SYBR Green PCR Master Mix, 10×miScript Universal Primer, and primers was incubated at 95°C for 15min, followed by 40 amplification cycles of 94°C for 10s, 55°C for 30s, and 70°C for 30s. The threshold cycle (Ct) was defined as the fractional cycle number at which the fluorescence passed the fixed threshold. Transcripts of U6 small RNA were quantified using the Hs_RNU6B_2 miScript Primer Assay (Qiagen, Hilden, Germany) for normalization of miRNA levels. The relative expression values were normalized to the internal control using 2^{-Ct}. The following primer sequences were used:

Human-miR-141-3p, 5'-TAACACTGTCTGGTAAAGATGG-3'

Human-miR-200a-3p, 5'-TAACACTGTCTGGTAACGATGT-3';

Western blotting assays

Whole-cell lysates were prepared according to the established procedures. Proteins were resolved by sodium dodecyl sulfateGmbH, Hrylamide gel electrophoresis, immunoblotted with the antibody of interest, and were visualized using an ECL chemiluminescence detection kit (Amersham Biosciences, Amersham, UK). At least three independent experiments were carried out with separate samples.

Cell culture in 3D ECM gels and time-lapse imaging

Three-dimensional (3D) collagen type I gel model was prepared using rat tail collagen type I (Corning). Collagen I mixtures (2.5 mg/ml) were prepared by adding the appropriate volumes of 10× reconstitution buffer (260 mM sodium bicarbonate and 200 mM HEPES) and 10× RPMI (Sigma Aldrich). To adjust the pH of the collagen solution to 7.2–7.4, an ice-cold solution of 2 N NaOH was used. The neutralized collagen solution was incubated on ice for 3-5 min to allow the pH to equilibrate, and then the solution was centrifuged at 10,000 g for 3 min at 4°C to eliminate air bubbles. Time-lapse DIC cell images were captured with an IX81-ZDC (Olympus, Japan) for 24 h at 37°C. The microscope was equipped with a Chamlide Incubator System (Live Cell Instrument, Korea), and the environmental chamber mounted on the microscope was constantly maintained at 37°C, 5% CO2, and 95% humidity.

3D immunofluorescence analysis

Cells were cultured within polydimethylsiloxane prepolymer (PDMS) glass coverslips (Song et al., 2017), and fixed directly with 4% formaldehyde for 30 min at room temperature and subsequently treated with 100 mM glycine to quench any residual aldehyde groups. After washing with PBS, the cells were permeabilized with 0.5% Triton X-100 for 30 min at RT and blocked for 2 h with PBS containing 3% BSA. In some cases, the cells were stained with either fluorescein-labeled phalloidin (Molecular Probes, 1:250) or Alexa Fluor® 488-labeled anti-cortactin (Millipore, 1:200) at 4°C overnight. The cells were then washed with wash buffer (130 mM NaCl, 13 mM Na2HPO4, and 3.5 mM NaH2PO4, pH 7.4). The nuclei were counterstained with Hoechst. Images were captured at 37°C using a confocal microscope with a Nikon Plan Apochromat 40× or

60×/1.4 N.A. oil objective (Nikon Eclipse Ti, Nikon, Japan) and analyzed using the NIS software (Nikon) or IMARIS imaging software (Bitplane AG, Zurich, Swiss). The confocal z-stack images obtained from NIS software were reconstructed into 3D images with the aid of the IMARIS software, Easy 3D mode. The visualization analysis of select images was performed using the ImarisColoc and Surpass module.

Statistical analysis

Statistically significant differences were assessed by the Student's t-test. The data were expressed as the mean ± SEM. Coefficients of correlation (r) were determined by the Pearson's correlation method. The Kaplan-Meier method was used for survival analysis. Statistical calculations of Pearson's correlation and Kaplan-Meier method were done using SPSS 20.0 and R.

Data availability

The data that support the findings of this study are available from the corresponding author upon reasonable request. All GEO data were from NCBI Gene Expression Omnibus (GEO accession number: GSE54236, GSE76427, GSE40367, GSE9843, and GSE94016).

Results (2,186 words)

Ινερσε ςορρελατιον βετωεεν ΕΡα ανδ Γα12 εξπρεσσιον

To investigate the relationship between the progression of HCC and ERα, we first analyzed a Gene Expression Omnibus (GEO) dataset including various stages of HCC tumors (GSE40637) and generated a heat map. Among the top five genes mostly upregulated as HCC progresses, we focused on Gα12 as a potential molecule affected by ERα (Fig. 1**A**). The result obtained from the STRING analysis showed the predicted interaction between *ESR1* and the genes from Fig. 1**A** that had significant changes as HCC progresses. Nonetheless, any direct interaction between ERα and Gα12 is yet unknown (Fig. 1**B**). Given the impact of increased Gα12 on the EMT and progression of HCC and elusive relationship between ERα and Gα12, we wondered whether sex difference affects GPCR activity. In Gene Set Enrichment Analysis (GSEA) using HCC human data (GSE 76427), gene sets associated with EMT and GPCR ligand binding showed significant enrichment in male patients with HCC (Fig. 1**C**). In particular, gene set termed as 'EMT' was the only significantly (FDR < 0.25) enriched gene sets in 'HALLMARK' (Supplementary 1). Indeed, the relationship between ERα and Gα12 may be the solution to understand the worsening of HCC, especially in males.

To extend this finding, we employed the GEO dataset in Fig. 1**A** and used Pearson correlation analysis to detect transcript levels. As expected, a strong negative relationship was revealed between *GNA12* and *ESR1,* but not between *GNA12* and *ESR2* or *G protein-coupled estrogen receptor 1 (GPER1)* (Fig. 1**D** , upper). Moreover, we confirmed that only *ESR1* was significantly decreased in metastatic HCCs (Fig. 1**D** , lower). On this basis, we analyzed the *GNA12* and *ESR1* from another GEO dataset and observed that *GNA12* mRNA levels were lower in patients presenting high levels of *ESR1* mRNA (Fig. 1**E**).

Ποορ συριαλ ρατε οφ Η™ πατιεντς ωιτη λοω ΕΡα ανδ ηιγη Γα12

After identifying the effect of ERα on HCC EMT via inverse relationship between Gα12, we then analyzed the effect of ERα on the survival rate of HCC patients (Supplementary Table 1), and found that a group of patients with low ERα and high Gα12 expression showed the poorest overall or recurrence-free survival rates; however, a group of high ERα and low Gα12 expression demonstrated the opposite effect. The cutoff for strong Gα12 intensity was set at '>3-fold' difference in HCC/NT$_{avg}$ (Fig. 2**A** , left and middle). Consistently, analysis of GEO dataset also showed the lowest overall survival rate with high Gα12 and low ERα, whereas those with low Gα12 and high ERα had the best outcomes (Fig. 2**A** , right). Next, we examined the expression of vimentin in the same samples and observed a significant negative association with *ESR1,* while detecting a positive correlation with *GNA12* (Fig. 2**B**).

Notably, we examined the ERα expression in the tumor section of tissues from HCC patients and found that ERα is lowly expressed while Gα12 is highly expressed compared with non-tumor section (Fig. 2**C**). Moreover, we used immunohistochemistry staining to compare ERα and Gα12 levels; ERα expression was

7

lower in tumorous tissues compared with non-tumorous tissues, consistent with an inverse relationship of high Gα12 expression in tumorous tissues (Fig. 2**D**). These results support that Gα12 expression is negatively correlated with ERα, suggesting patients with higher ERα have higher overall survival and recurrence-free survival rates, proposing a possible protective role of ERα in HCC progression.

Τρανσςριπτιοναλ ινηιβιτιον οφ Γα12 βψ ΕΡα αςτιατιον

To elucidate the underlying effect of ERα on HCC progression via Gα12, we incorporated a 'Tet-On system' to establish a stable cell line that selectively expresses ERα (Fig. 3**A** , left). As expected, treatment of Tet O-ERα cells with doxycycline (Dox) decreased Gα12 mRNA levels (Fig. 3**A** , right and Supplementary 2**A**). Since the classical mechanism of ERα action involves estrogen binding to receptors in the cell and the activated ERα binds to specific response elements known as estrogen response elements (EREs) located in target genes. To corroborate the role of ERα in regulating Gα12 transcription, qRT-PCR was performed to assess the effect of modulating ERα expression at the level of Gα12 mRNA. Using an ERα overexpression vector, we demonstrated that overexpression of ERα induced the downregulation of Gα12 in SNU449 cells (Fig. 3**B** , left and Supplementary 2**B**). Silencing endogenous ERα by using siRNAs led to an upregulation of Gα12 in HepG2 cells (Fig. 3**B** right and Supplementary 2**B**). Furthermore, in SNU387 cells treated with E2 time-dependently, the inhibitory effect was found since *GNA12*mRNA levels were significantly decreased (Fig. 3**C**).

To validate the inhibitory effect of ERα on *GNA12* , we sought an ERE binding site within the *GNA12* promoter. Using the ChIP assay, we observed that ERα is a novel inhibitory regulator of Gα12 (Fig. 3**D**). The luciferase activity assay confirmed that ERα binds to the Gα12 promoter region. A wildtype *GNA12* promoter-luciferase vector was transfected in HEK293A cells and ectopic overexpression of ERα significantly decreased the *GNA12* promoter activity (Fig. 3**E**). Lastly, using an immunocytochemistry assay, we found that Dox and E2 treatment significantly inhibited Gα12 expression in HCC cells (Fig. 3**F**). These results indicate that ERα directly inhibits the transcription of Gα12.

ΕΡα ινηιβιτιον οφ ΕΜΤ βιομαρκερς

To consolidate the role of ERα in suppressing Gα12 and EMT, immunoblottings were done to demonstrate the suppression of Gα12 and EMT related proteins (vimentin, zinc finger E-box-binding homeobox 1 (ZEB1), and epithelial cadherin (E-cadherin)) (Fig. 4**A**). Furthermore, we confirmed the inhibitory effect of ERα on Gα12 and EMT by showing that the inhibitory effect of Gα12 and EMT was suppressed when Gα12 was overexpressed (Fig. 4**B**). Additionally, the expression levels of ERα and Gα12/EMT marker proteins were examined using transient and stable ERα transfection (Fig. 4**C**). Inversely, ERα silencing increased the levels of Gα12 and EMT markers (Fig. 4**D**).

We further demonstrated the suppression of Gα12 and other EMT markers in the female-derived cell line SNU387 time-dependently (Fig. 4**E**). Consistently, treatment with fulvestrant (ICI 182,780), an antagonist of E2 and ERα down-regulator, promoted the expression of Gα12 and EMT markers (Fig. 4**F**). We corroborated the association between ERα and EMT by measuring their endogenous protein levels in several cell lines; mesenchymal-typed HCC cells (SK-Hep1 and SNU449) exhibited lower levels of ERα when compared with epithelial-typed cells (Huh7 and HepG2). Also, SNU387 was used as a positive control as it is a female mesenchymal-typed HCC cell (Fig. 4**G**). Our results show that ERα suppression of EMT results from Gα12 inhibition.

Ιδεντιφιςατιον οφ ΠΤΠ4Α1 ας α ταργετ μολεςυλε οφ μιΡ-141 ανδ μιΡ-200α, ρεγυλατεδ βψ ΕΡα/ Γα12

To dissect the mechanism of how the ERα/Gα12 axis can alter HCC progression, we focused on miRNAs as potential downstream molecules. First, our laboratory previously has performed microarray analyses to assess alterations in miRNA expression in Gα12QL-Huh7 cells and found downregulated and upregulated miRNAs by Gα12 (Yang et al., 2015). Here, Gα12QL indicates a consistently active mutant form of Gα12. Then, common miRNAs were sorted from the list of miRNAs upregulated by estrogen (Huang et al., 2015; Cohen and Smith, 2014) and downregulated by Gα12 overexpression. Surprisingly, only two miRNAs were controlled

8

by the ERα-Gα12 axis: miR-141 and -122 (Fig. 5**A**). We selected miR-141 for further investigations as miR-122 did not express gender disparity while miR-141 did in our human samples (Supplementary 3**A** and Fig.7**C**). We then found that miR-200a presented the same seed sequences as miR-141 (Kehl et al., 2017).

To investigate whether the screened miRNAs are undoubtedly regulated by ERα-Gα12, we used the HCC cell line stably transfected with an ERα overexpression vector and validated the upregulation of miR-141 and -200a (Fig. 5**B** , left). In contrast, ERα was silenced using siRNA, downregulating miR-141 and -200a in HepG2 cells (Fig. 5**B** , right). Similar results were obtained using another cell line; SNU387 treated with E2 indicated increased level of miR-141 and -200a (Fig. 5**C**).

In Fig. 5**D** , we found that when Gα12 is silenced (Supplementary 4**A**), miR-141 and -200a levels increase. Finally, we used Tet-O-ERα cells to transfect the Gα12 overexpression vector and simultaneously modulated ERα and Gα12. The reinforced expression of Gα12 prevented ERα overexpression from increasing miR-141 and -200a (Fig. 5**E**). Hence, ERα may regulate miR-141 and -200a through suppression of Gα12.

Having identified the effect of ERα-Gα12 on miR-141 and -200a, we investigated the target of miR-141 and -200a, a protein possibly implicated in the aggressiveness of HCC. We used Targetscan, a bioinformatics analysis tool, to select the putative targets regulated by miR-141 and -200a. Among the 500 putative targets generated, we did cluster analysis using gene ontology and selected the pathway that regulates cell migration (Supplementary 4**B**). Protein tyrosine phosphatase 4A1 (PTP4A1) was chosen for further analysis since phosphatases are emerging therapeutic targets and the role of PTP4A1 in migration and invasion is well known but the regulator is yet elusive (Fig. 5**F**). Then, we found a putative binding site of miR-141 and -200a at the 3'UTR of PTP4A1 mRNA (Fig. 5**G** , left). We next used the luciferase assay to confirm the binding of miR-141 and 200a and PTP4A1 3'UTR region (Fig. 5**G** , left). As miRNAs may degrade target proteins (Bartel, 2004), we investigated the possibility of PTP4A1 mRNA regulation, which failed to show significant changes due to ERα modulation (Supplementary 4**D**). To confirm the role of miR-141 and -200a in regulating PTP4A1 in the ERα/Gα12 axis, *in vitro* assays were done after enhancing or silencing the miRNA and ERα/Gα12. Transfection with miR-141 and -200a mimic or antisense oligonucleotide (ASO) did not influence PTP4A1 mRNA (Supplementary 4**C**). Furthermore, miR-141 and -200a mimic decreased PTP4A1 protein levels while ASO increased PTP4A1 protein levels (Fig. 5**G** , right). Consistently, ERα overexpression decreased PTP4A1, whereas ERα silencing increased PTP4A1 (Fig. 5**H**). Moreover, the effect of ERα and Gα12 on PTP4A1 was confirmed through western blotting (Fig. 5**I**). In addition, modulation of PTP4A1 on HCC cells affected EMT markers (Fig. 5**J**). These results demonstrated that miR-141 and -200a directly inhibits PTP4A1 translation by targeting the 3' UTR region.

Ρολε οφ ΕΡα ανδ Γα12 ον amoeboid motility

When cancer cells migrate, they have two types of mode: mesenchymal and amoeboid (Sahai and Marshall, 2003), as shown in Fig. 6**A** . The amoeboid features include membrane blebbing, cell rounding, and increased invasion (Poincloux et al., 2011; Liu et al., 2015; Crosas-Molist et al., 2017). After identifying the link between miR-141/-200a and PTP4A1, as well as the effects of PTP4A1 on its role in HCC progression, we attempted to find whether ERα regulates mesenchymal-amoeboid transition (MAT). Through the analysis of GSEA (GSE9843), we were able to discover many MAT-related pathways increased in male HCC patients (Fig. 6**B** , Supplementary 5).

Then, we analyzed the morphology and blebbing of SK-Hep1 cell population, presenting both control and ERα overexpression, in the 3D matrix using live-cell imaging technique (Fig. 6**C**). In the 3D environment, the migration of invasive SK-Hep1 cells showed less blebbing following the overexpression of ERα. To confirm the effect of ERα on amoeboid-blebbing behavior, we examined the levels of the active form of myosin light chain (Ser19) (p-MLC), an amoeboid gold standard marker, in SK-Hep1 cells modulating ERα. The confocal assay showed increased expression of p-MLC, as well as its rear distribution (Fig. 6**D**), promoting amoeboid movement in the vehicle group (Wilkinson et al., 2005). Next, we examined the protein level of p-MLC by controlling ERα expression. Bona fide, ERα overexpression suppressed p-MLC, whereas siERα increased p-MLC (Fig. 6**E**). Moreover, the overexpression of Gα12 prevented ERα from inhibiting p-MLC levels

9

(Fig. 6**F**). Thus, ERα negatively regulates MLC phosphorylation and thereby actomyosin contractility and increased cell migration. Since RhoA/ROCK is a well-established molecule that phosphorylates MLC, and is a downstream molecule of Gα12 (Hart et al., 1998), we postulated that p-MLC may be a functional molecule under the control of ERα/Gα12 axis.

Changes in PTP4A1, p-MLC, and miRNAs in xenograft animal dataset and human samples

In the analysis of publicly available GEO dataset (Yang et al., 2018), the *ESR1* level decreased under the situation of metastasis, whereas *GNA12* and *PTP4A1* increased. We confirmed the negative relationships between *ESR1* and *GNA12* (or*PTP4A1*) using Pearson correlation analysis (Fig. 7**A**).

To further explore the relationship between ERα/Gα12 and the target molecules, we did immunoblottings for PTP4A1 and p-MLC. Respectively, samples of tumorous regions showed significantly elevated PTP4A1 and p-MLC levels (Fig. 7**B**). Additionally, we observed the histological expression of these molecules in HCC patients, revealing similar results. PTP4A1 and p-MLC expression showed an inverse relationship with ERα while showed a positive relationship with metastatic proteins (Vimentin and Gα12) (Fig. 7**C**).

To associate the above *in vitro* results with human HCC progression and further explain the gender disparity, we did qRT-PCR assays for miR-141 and -200a. These miRNAs show positive correlations with ESR1 mRNA levels in HCC patients (Fig. 7**D** , left). Also, miR-141 and -200a were significantly elevated in female patients (Fig. 7**D** , right). Furthermore, males demonstrated higher Gα12, PTP4A1 and p-MLC levels when compared with those observed in females (Fig. 7**E**). As the expression of ERα in males was one-fifth of that expressed in females (Cooke et al., 2017), the suppression of Gα12 would be inhibited. Consequently, miR-141 and -200a were downregulated, and inversely PTP4A1 was increased. In addition, p-MLC was activated as Gα12 activates RhoA/ROCK/MLC (Fig. 7**F**).

Discussion (1,355 words)

The incidence of HCC varies worldwide; however, in almost all populations, the male to female ratio averages between 2:1 and 4:1 (Fitzmaurice et al., 2017). HCC is a complex heterogeneous tumor with many genomic alterations (Cancer Genome Atlas Research Network, 2017). To overcome this complexity, an effective combination of molecular therapies is crucial. In addition, the sex bias and consequent changes in major biomarkers suggest the need for personalized therapy (Natri et al., 2019). There is a report indicating that estrogen ameliorates HCC through inhibition of IL-6/STAT3 in Kupffer cells (Stein and Yang, 1995). Furthermore, several reports have revealed the association between certain cancer progression and ERα. Nevertheless, the targets explaining the gender disparity of HCC incidence and worsening remain elusive. In this study, we report that inhibition of Gα12 signaling by ERα leads to the suppression of key aspects of both mesenchymal and amoeboid migration in HCC cells, resulting in substantial hinderance on cell motility.

Gα12 is known to induce EMT of HCC (Yang et al., 2015), regulating pathways associated with the enhancement of pro-metastatic genes (Heo et al., 2014). In the present study, we demonstrated that ERα repressed the expression of Gα12. Moreover, higher ERα and lower Gα12 levels account for the longer survival and lower recurrence rate. Consistently, human HCC samples have shown lower levels of ERα in HCC than in NT (Yang et al., 2015).

Deregulation of miRNAs is involved in cancer malignancy, particularly liver tumor EMT (Zaravinos, 2015). In our findings, miR-141 and -200a belonged to miRNAs exclusively regulated by both ERα and Gα12 during HCC progression. miR-141 and -200a are known to regulate cancer growth and metastasis (Huang et al., 2017; Pichler et al., 2014; Li et al., 2019). Importantly, HCC cells have demonstrated increased levels of miR-141 and -200a, presenting higher expression levels in females than in males. Other molecules targeted by miR-141 and -200a are clustered into several pathways such as actin nucleation and chromosome organizations, irrelevant in our study (Supplementary 4**B**).

PTP4A1 plays a role in cell proliferation and migration, cell cycle progression, and cell motility and invasion (Li et al., 2014). PTP4A1 has two other isoforms, PTP4A2, and PTP4A3, which have similar functions (Liu et al., 2016). Oncogenic PTP4A1 contains a phosphatase domain which is essential for tumor cell

10

metastasis and affects focal adhesion regulation (Rios et al., 2013). PTP4A1 regulates miR-601 in breast cancer metastasis (Bai et al., 2011). In this context, the regulation of EMT remains pivotal. Furthermore, it functions in the TGF-β pathway, contributing to fibrosis and systemic sclerosis (Hu et al., 2016). The results shown in this study support the notion that Gα12 modulates PTP4A1 and is affected by ERα. Therefore, through ERα and Gα12, EMT phenotype is inhibited. An improved understanding of the functions and regulatory mechanism of PTP4A1 may lead to new considerations of this protein as a biomarker or therapeutic target for HCC.

In the current study, another interesting finding involves the identification of PTP4A1 as a target of miR-141 and -200a. Indeed, PTP4A1 appeared to be a specific target of miR-141 and -200a, supporting the hypothesis that the miRNAs contribute to the suppression of HCC progression through PTP4A1. Consistently, the outcomes of our cell-based assays support the idea that the miRNAs were upregulated by ERα ligand treatment through Gα12 repression, but were downregulated by Gα12 overexpression. Although the miRNAs share identical seed sequences, miR-200a is more known to play a role in cell motility (Wang et al., 2014). Interestingly, PTP4A1 seems to respond more strongly to miR-200a than miR-141. We corroborated the effects of PTP4A1 modulations on EMT. Additionally, there are other miRNAs down-regulated by Gα12 in HCC. Among them, 15 miRNAs are known to be downregulated in HCC, 4 are related to HCC apoptosis, 6 are related to angiogenesis, and 11 are related to invasion, EMT, and HCC metastasis (Xu et al., 2018). It remains to be investigated whether the targets are regulated by Gα12.

Cancer cells can take another mode of motility, characterized as amoeboid movement (Sahai and Marshall, 2003). Amoeboid movement promotes tumor progression and is used to reprogram the immune microenvironment, another important factor in cancer metastasis (Vaškovičová et al., 2015; Georgouli et al., 2019). According to Lehmann et al. , cells undergoing amoeboid movement carry EMT signatures for dissemination from the epithelial tumor. The amoeboid profile alone is insufficient to present metastasis as it is difficult to distinguish mesenchymal and amoeboid movements (Garner and de Visser, 2020). There is growing evidence focusing on the dual targeting of mesenchymal and amoeboid movements (Vaškovičová et al., 2015; Jones et al., 2017). However, limited studies have investigated amoeboid movement, especially in the field of HCC. It would be necessary to inhibit both mesenchymal and amoeboid migration and invasion for efficient therapy (Jones et al., 2017).

The gender disparity observed in HCC prognosis could be explained by differences in p-MLC, a amoeboid marker, along with alterations in PTP4A1, which may account for the metastatic capability. Indeed, the SK-Hep1 cell model that we used for our invasion/migration assays showed strong invasive power (data not shown). Hence, we were unable to differentiate alterations in cell movement in the experiment modulating ERα and Gα12, to observe the effect of invasion and migration assays (Sacchetti et al., 2017). However, our results support the possibility that Gα12 under the control of ERα modulates the p-MLC level, which may explain gender disparity in HCC exacerbation; this observation was supported by outcomes of the amoeboid cell movement video assay (Supplementary Movie 1-4).

Among molecules associated with amoeboid movement, NOX4 inhibits the transition of HCC cells to amoeboid cells and suppresses tumor dissemination (Crosas-Molist et al., 2017). CD147 promotes Src-dependent activation of Rac1 signaling during the motility of HCC (Lehmann et al., 2017). It has been proposed that simultaneous inhibition of ROCK and NEDD9 additionally decreased breast cancer cell migration and invasion (Jones et al., 2017). ROCK is one of the main downstream molecules of the Gα12 pathway and is known to facilitate a switch to amoeboid motility (Seasholtz et al., 1999; Matsuoka and Yashiro, 2014). The results showing inhibition of amoeboid cell migration and invasion by ERα through the Gα12 pathway, suggest an efficient approach clarifying HCC progression.

To elucidate the pathogenesis of HCC and investigate the effects of potential targets, mouse models, especially subcutaneous xenograft models, have been proposed as a useful tool (He et al., 2015). Previously, we have used a subcutaneous xenograft model to demonstrate that Gα12 knockdown diminishes the overall growth rate (Yang et al., 2015). Here, we performed an in-depth effort to implement SK-Hep1 Tet O-ERα cells into SCID mice, despite which, tumor formation failed. The specific error was reportedly the attempt to

11

establish solid tumors (100 cm^3) after implanting SK-Hep1 Tet O-ERα cells using Charles River Balb/c nude mouse and JoongAh Bio NRGA mouse. However, HCC mouse models often experience limitations such as interference of cell growth by varied size and heterogeneity of constructs (Bi et al., 2019). Nonetheless, our analysis of the public dataset derived from a xenograft mouse model supports *in vivo* validity of the proposed pathway (Fig. 7**A**).

Estrogen replacement therapy (ERT) is a treatment that replaces the role of hormones with medication therapy (Collaborative Group on Hormonal Factors in Breast Cancer, 2019). ERT is important to prevent later health conditions (Biglia et al., 2017). ERT may pose risks including an increase in breast cancer. However, the incidence of colorectal cancer decreases (Rossouw et al., 2002). Our findings delineate the molecular pathway of ERα regulation of Gα12 through the miR141/200a network. Moreover, the identified molecules displayed gender differences, suggestive of the role of ERα in explaining significantly low mortality in females and possible applications of estrogen. Moreover, our findings support the significance of ERα and Gα12 as independent prognostic factors for tumor recurrence so that the molecules and signaling axis are beneficial in understanding sex differences in HCC incidence and malignant progression. In addition, the resultant changes in amoeboid plasticity of cancer cells may explain HCC aggravation in males, and consequent better survival rates observed in females, supporting the idea that modulating the ERα-Gα12 pathway may be utilized for sex differential approaches in HCC treatment.

References

1. Bai, Y., Luo, Y., Liu, S., Zhang, L., Shen, K., Dong, Y., . . . Zhang, Z. Y. (2011). PRL-1 protein promotes ERK1/2 and RhoA protein activation through a non-canonical interaction with the Src homology 3 domain of p115 Rho GTPase-activating protein. *The Journal of Biological Chemistry* , 286, 42316–42324.
2. Barreca T, Picciotto A, Franceschini R, Varagona G, Garibaldi A, Valle F, . . . Rolandi E. (1993). Sex hormones and sex hormone-binding globulin in males with chronic viral hepatitis during recombinant interferon-alpha 2b therapy. *J Interferon Res,* 13, 209– 211.
3. Bartel D. P. (2004). MicroRNAs: genomics, biogenesis, mechanism, and function. *Cell* , 116, 281–297.
4. Bi, Y., Shi, J., Li, S., Wang, Q., Wang, Q., Wen, X., . . . Feng, H. (2019). A novel xenograft model of human HCC in immunocompetent mouse.*BioRxiv,* http://doi: https://doi.org/10.1101/762351.
5. Biglia N, Cagnacci A, Gambacciani M, Lello S, Maffei S, Nappi RE. (2017). Vasomotor symptoms in menopause: a biomarker of cardiovascular disease risk and other chronic diseases. *Climacteric,* 20, 306-312.
6. Bigsby RM. and Caperell-Grant A. (2011). The role for estrogen receptor-α and prolactin receptor in sex-dependent DEN-induced liver tumorigenesis. *Carcinogenesis* , 32, 1162– 1166.
7. Bray, F., Ferlay, J., Soerjomataram, I., Siegel, R.L., Torre, L.A. and Jemal, A. (2018). Global cancer statistics 2018: GLOBOCAN estimates of incidence and mortality worldwide for 36 cancers in 185 countries.*A Cancer Journal for Clinicians* , 68, 394-424.
8. Cancer Genome Atlas Research Network (2017). Comprehensive and Integrative Genomic Characterization of Hepatocellular Carcinoma.*Cell,* 169, 1327–1341.
9. Choi, S. S. and Diehl, A. M. (2009). Epithelial-to-mesenchymal transitions in the liver. *Hepatology,* 50, 2007–2013.
10. Cohen, A. and Smith, Y. (2014). Estrogen regulation of microRNAs, target genes, and microRNA expression associated with vitellogenesis in the zebrafish. *Zebrafish,* 11, 462–478.
11. Collaborative Group on Hormonal Factors in Breast Cancer (2019). Type and timing of menopausal hormone therapy and breast cancer risk: individual participant meta-analysis of the worldwide epidemiological evidence. *Lancet* , 394, 1159–1168.
12. Cooke, P. S., Nanjappa, M. K., Ko, C., Prins, G. S., and Hess, R. A. (2017). Estrogens in Male Physiology. *Physiological Reviews* , 97, 995–1043.
13. Crosas-Molist, E., Bertran, E., Rodriguez-Hernandez, I., Herraiz, C., Cantelli, G., Fabra, À., . . . Fabregat, I. (2017). The NADPH oxidase NOX4 represses epithelial to amoeboid transition and efficient tumour dissemination. *Oncogene* , 36, 3002–3014.

14. Fitzmaurice, C., Allen, C., Barber, R. M., Barregard, L., Bhutta, Z. A., Brenner, H., . . . Mohsen, N. (2017). Global, regional, and national cancer incidence, mortality, years of life lost, years lived with disability, and disability-adjusted life-years for 32 cancer groups, 1990 to 2015: A systematic analysis for the global burden of disease study. *JAMA Oncology,* 3, 524–548.

15. Garner, H. and de Visser, K. E. (2020). Immune crosstalk in cancer progression and metastatic spread: a complex conversation.*Nature Reviews. Immunology,* 10.1038/s41577-019-0271-z.

16. Georgouli, M., Herraiz, C., Crosas-Molist, E., Fanshawe, B., Maiques, O., Perdrix, A., . . . Sanz-Moreno, V. (2019). Regional Activation of Myosin II in Cancer Cells Drives Tumor Progression via a Secretory Cross-Talk with the Immune Microenvironment. *Cell,* 176, 757–774.e23.

17. Hart, M. J., Jiang, X., Kozasa, T., Roscoe, W., Singer, W. D., Gilman, A. G., . . . Bollag, G. (1998). Direct stimulation of the guanine nucleotide exchange activity of p115 RhoGEF by Galpha13.*Science* , 280, 2112–2114.

18. He, L., Tian, D. A., Li, P. Y., and He, X. X. (2015). Mouse models of liver cancer: Progress and recommendations. *Oncotarget,* 6, 23306.

19. Heo, M. J., Kim, Y. M., Koo, J. H., Yang, Y. M., An, J., Lee, S. K., . . . Kim, S. G. (2014). microRNA-148a dysregulation discriminates poor prognosis of hepatocellular carcinoma in association with USP4 overexpression. *Oncotarget,* 5, 2792–2806.

20. Hu, J. Y., Yi, W., Wei, X., Zhang, M. Y., Xu, R., Zeng, L. S., . . . Chen, J. S. (2016). miR-601 is a prognostic marker and suppresses cell growth and invasion by targeting PTP4A1 in breast cancer. *Biomedicine & Pharmacotherapy,* 79, 247–253.

21. Huang, F. Y., Wong, D. K., Seto, W. K., Lai, C. L., and Yuen, M. F. (2015). Estradiol induces apoptosis via activation of miRNA-23a and p53: implication for gender difference in liver cancer development.*Oncotarget,* 6, 34941–34952.

22. Huang, S., Wa, Q., Pan, J., Peng, X., Ren, D., Huang, Y., . . . Tang, Y. (2017). Downregulation of miR-141-3p promotes bone metastasis via activating NF-ϰB signaling in prostate cancer. *Journal of Experimental & Clinical Cancer Research,* 36, 173.

23. Jones, B. C., Kelley, L. C., Loskutov, Y. V., Marinak, K. M., Kozyreva, V. K., Smolkin, M. B., and Pugacheva, E. N. (2017). Dual Targeting of Mesenchymal and Amoeboid Motility Hinders Metastatic Behavior. *Molecular Cancer Research,* 15, 670–682.

24. Kehl, T., Backes, C., Kern, F., Fehlmann, T., Ludwig, N., Meese, E., . . . Keller, A. (2017). About miRNAs, miRNA seeds, target genes and target pathways. *Oncotarget,* 8, 107167–107175.

25. Lehmann, S., Te Boekhorst, V., Odenthal, J., Bianchi, R., van Helvert, S., Ikenberg, K., . . . Friedl, P. (2017). Hypoxia Induces a HIF-1-Dependent Transition from Collective-to-Amoeboid Dissemination in Epithelial Cancer Cells. *Current Biology* , 27, 392–400.

26. Li, H., Tang, J., Lei, H., Cai, P., Zhu, H., Li, B., . . . Tang, W. (2014). Decreased MiR-200a/141 suppress cell migration and proliferation by targeting PTEN in Hirschsprung's disease.*Cellular Physiology and Biochemistry* , 34, 543–553.

27. Li, W., Cui, Y., Wang, D., Wang, Y., and Wang, L. (2019). MiR-141-3p functions as a tumor suppressor through directly targeting ZFR in non-small cell lung cancer. *Biochemical and Biophysical Research Communications,* 509, 647–656.

28. Liu, L. Z., He, Y. Z., Dong, P. P., Ma, L. J., Wang, Z. C., Liu, X. Y., . . . Wang, X-Y. (2016). Protein tyrosine phosphatase PTP4A1 promotes proliferation and epithelial-mesenchymal transition in intrahepatic cholangiocarcinoma via the PI3K/AKT pathway.*Oncotarget,* 7, 75210–75220.

29. Liu, W. H., Yeh, S. H., Lu, C. C., Yu, S. L., Chen, H. Y., Lin, C. Y., . . . Chen, P. J. (2009). MicroRNA-18a prevents estrogen receptor-alpha expression, promoting proliferation of hepatocellular carcinoma cells. *Gastroenterology* , 136, 683-693.

30. Liu, Y. J., Le Berre, M., Lautenschlaeger, F., Maiuri, P., Callan-Jones, A., Heuzé, M., . . . Piel, M. (2015). Confinement and low adhesion induce fast amoeboid migration of slow mesenchymal cells.*Cell,* 160, 659–672.

31. Matsuoka T. and Yashiro M. (2014). Rho/ROCK signaling in motility and metastasis of gastric cancer. *World J Gastroenterol,* 20, 13756-13766.

13

32. Natri, H. M., Wilson, M. A., and Buetow, K. H. (2019). Distinct molecular etiologies of male and female hepatocellular carcinoma.*BMC Cancer,* 19, 951.

33. Naugler, W. E., Sakurai, T., Kim, S., Maeda, S., Kim, K., Elsharkawy, A. M., and Karin, M. (2007). Gender disparity in liver cancer due to sex differences in MyD88-dependent IL-6 production. *Science,*317, 121–124.

34. Nieto MA. (2013). Epithelial plasticity: a common theme in embryonic and cancer cells. *Science,* 342, 1234850.

35. Nobes, C. D., and Hall, A. (1995). Rho, rac, and cdc42 GTPases regulate the assembly of multimolecular focal complexes associated with actin stress fibers, lamellipodia, and filopodia. *Cell,*81, 53–62.

36. Pankova, K., Rosel, D., Novotny, M., and Brabek, J. (2010). The molecular mechanisms of transition between mesenchymal and amoeboid invasiveness in tumor cells. *Cellular and Molecular Life Sciences,* 67, 63–71.

37. Pichler, M., Ress, A. L., Winter, E., Stiegelbauer, V., Karbiener, M., Schwarzenbacher, D., . . . Hoefler, G. (2014). MiR-200a regulates epithelial to mesenchymal transition-related gene expression and determines prognosis in colorectal cancer patients. *British Journal of Cancer,* 110, 1614–1621.

38. Poincloux, R., Collin, O., Lizarraga, F., Romao, M., Debray, M., Piel, M., and Chavrier, P. (2011). Contractility of the cell rear drives invasion of breast tumor cells in 3D Matrigel. *Proceedings of the National Academy of Sciences of the United States of America* , 108(5), 1943–1948.

39. Rios, P., Li, X., and Kohn, M. (2013). Molecular mechanisms of the PRL phosphatases. *The FEBS Journal* , 280(2), 505–524.

40. Rossouw JE, Anderson GL, Prentice RL, LaCroix AZ, Kooperberg C, Stefanick ML, . . . Writing Group for the Women's Health Initiative Investigators. (2002). Risks and benefits of estrogen plus progestin in healthy postmenopausal women: principal results from the Women's Health Initiative randomized controlled trial. *JAMA* , 288, 321-333.

41. Sacchetti, C., Bai, Y., Stanford, S. M., Di Benedetto, P., Cipriani, P., Santelli, E., . . . Bottini, N. (2017). PTP4A1 promotes TGFβ signaling and fibrosis in systemic sclerosis. *Nature Communications,* 8(1), 1060.

42. Sahai, E., and Marshall, C. J. (2003). Differing modes of tumour cell invasion have distinct requirements for Rho/ROCK signalling and extracellular proteolysis. *Nature Cell Biology,* 5(8), 711–719.

43. Seasholtz, T. M., Majumdar, M., and Brown, J. H. (1999). Rho as a mediator of G protein-coupled receptor signaling. *Molecular Pharmacology,* 55(6), 949–956.

44. Song, D. G., Lee, G. H., Nam, S. H., Cheong, J. G., Jeong, D., Lee, S. J., . . . Lee, J.W. (2017). TM4SF5 promotes metastatic behavior of cells in 3D extracellular matrix gels by reducing dependency on environmental cues. *Oncotarget,* 8(48), 83480-83494.

45. Stein, B. and Yang, M. X. (1995). Repression of the interleukin-6 promoter by estrogen receptor is mediated by NF-kappa B and C/EBP beta. *Molecular and Cellular Biology,* 15(9), 4971–4979.

46. Thiery J, Acloque H, Huang R, and Nieto M. (2009). Epithelial-mesenchymal transitions in development and disease.*Cell,* 139(5), 871–90.

47. Vaškovičová, K., Szabadosová, E., Čermák, V., Gandalovičová, A., Kasalová, L., Rösel, D., and Brábek, J. (2015). PKCα promotes the mesenchymal to amoeboid transition and increases cancer cell invasiveness. *BMC Cancer,* 15, 326.

48. Wang S., Cui H., Liu Y., Zhao P., Zhang Y., Fu Z., . . . Jiang J. (2014). CD147 promotes Src-dependent activation of Rac1 signaling through STAT3/DOCK8 during the motility of hepatocellular carcinoma cells. *Oncotarget,* 6, 243-257.

49. Wilkinson, S., Paterson, H. F., and Marshall, C. J. (2005). Cdc42-MRCK and Rho-ROCK signalling cooperate in myosin phosphorylation and cell invasion. *Nature Cell Biology,* 7(3), 255–261.

50. Wu, H., Yao, S., Zhang, S., Wang, J. R., Guo, P. D., Li, X. M., . . . Li, J. M. (2017). Elevated expression of Erbin destabilizes ERα protein and promotes tumorigenesis in hepatocellular carcinoma.*Journal of Hepatology,* 66(6), 1193–1204.

51. Xu, X., Tao, Y., Shan, L., Chen, R., Jiang, H., Qian, Z., . . . Yu, Y. (2018). The Role of MicroRNAs in Hepatocellular Carcinoma.*Journal of Cancer,* 9(19), 3557–3569.

52. Yang, B., Li, M., Tang, W., Liu, W., Zhang, S., Chen, L., and Xia, J. (2018). Dynamic network biomarker indicates pulmonary metastasis at the tipping point of hepatocellular carcinoma. *Nature Communications,* 9(1), 678.

53. Yang, W., Lu, Y., Xu, Y., Xu, L., Zheng, W., Wu, Y., . . . Shen, P. (2012). Estrogen represses hepatocellular carcinoma (HCC) growth via inhibiting alternative activation of tumor-associated macrophages (TAMs). *Journal of Biological Chemistry,* 287(48), 40140–40149.

54. Yang, Y. M., Lee, W. H., Lee, C. G., An, J., Kim, E. S., Kim, S. H., . . . Kim, S. G. (2015). Gα12 gep oncogene deregulation of p53-responsive microRNAs promotes epithelial-mesenchymal transition of hepatocellular carcinoma. *Oncogene* , 34(22), 2910–2921.

55. Zaravinos A. (2015). The Regulatory Role of MicroRNAs in EMT and Cancer. *Journal of Oncology,* 2015, 865816.

Figure legends

Figure 1. Inverse correlation between ERα and Gα12 expression in HCC

(A) Heat map showing significantly increased and decreased mRNAs across the progression of HCC using the GEO database (GSE40367; Roessler S.*et al.* , 2012) and KEGG pathway: pathways in cancer. Colors represent log2 gene expression fold change in normal controls when compared with non-metastatic HCC and metastatic HCC patients. A log2 fold change of more than 2 or less than -2 was considered overexpression or suppression (blue, underexpression; white, no change; and red, overexpression; n =5 for normal, n =10 for non-metastatic HCC, and n =20 for metastatic HCC).

(B) An interaction map of *ESR1* and highly changed genes from HCC progression. A gene interaction network of *ESR1* and genes from panel (A), revealing the unidentified interaction between *GNA12* and *ESR1* using a biological database STRING. The interaction map is drawn using Cytoscape. Each line indicates known and predicted association.

(C) GSEA-enrichment plots showing enriched signaling pathways in males (versus females) HCC patients (GSE76427; Grinchuk OV, *et al.* , 2018). Gene sets involved in EMT hallmark (*left*) and GPCR ligand binding receptor were positively correlated with HCC males (*right* , n = 21 females, and 94 males) (*left* , NES =1.61, FDR <0.25; *right* , NES =2.28, FDR <0.25).

(D) Pearson correlation analyses showing negative relationship between*GNA12* and estrogen receptor isoforms. (*Upper*) Using human HCC GEO dataset from Fig. 1A, correlations between estrogen receptors*ESR1* , *ESR2* , and *GPER1* and *GNA12* were investigated. Correlations were analyzed by Pearson correlation analysis (r). Each point represents one sample, and the horizontal line indicates the mean value (n =35). (*Lower*) Moreover, screened for relationships between estrogen receptors (*ESR1* , *ESR2* , and*GPER1*) in HCC patients with or without metastasis (or normal controls) deposited in GEO database (GSE40367, Roessler S. *et al.* , 2012) (n =5 for normal, n =10 for non-metastatic HCC, and n =20 for metastatic HCC). The horizontal line indicates the mean value. Data were analyzed using the ANOVA.

(E) Relationship between *GNA12* and *ESR1* in patients with HCC using the GEO dataset (GSE54236, Villa E. *et al.* , 2016). The samples were divided into two groups of high and low gene expression according to qRT-PCR assay results for *GNA12* and *ESR1* . The cutoff for high low expression was defined by the median. The data were analyzed using the Chi-square test.

Figure 2. Survival rates of patients with HCC in association with ERα and Gα12 expression

(A) Kaplan-Meier analyses of HCC patients. The overall survival curves and recurrence free survival rates of HCC patients from Asan Medical Center (*left* , n =59) and in HCC GEO database (*right* , GSE76427, Grinchuk OV, *et al.* , 2018) in terms of Gα12 and ERα expression (n =21 females, and 94 males). HCC patients are grouped by high ERα and low Gα12, or low ERα and high Gα12 expression. The cutoff for strong Gα12 intensity was set at a '>3-fold' difference in human tumourous HCC (T) / non-tumorous (N)$_{avg}$. P-value was generated by the log-rank test.

(B) Pearson correlation analyses to explore relationship among *ESR1* and EMT related genes, *GNA12* and *VIM* . HCC patients. *ESR1* and *VIM* (*left*), and *VIM* and *GNA12* using GEO database (GSE40367, Roessler S.*et al.* , 2012) (*right* , n =35). Correlations were analyzed by using pearson correlation analysis (r). Each point represents one sample.

(C) Immunoblottings for Gα12 and ERα in T and N samples. Protein levels were measured in 59 pairs of primary Ts and Ns. *p<0.05 and ***p<0.001. Data were analyzed using the two-tailed Student's t-test.

(D) IHC for ERα and Gα12 (x 200). ERα and Gα12 protein levels were analyzed by IHC in T tissues (versus N tissues). (n =3, 4-5 replicates/group for each experiment, Scale bar, 200 μm). Pictures are representative images. *p<0.05 and **p<0.01. Data were analyzed using the two-tailed Student's t-test.

Figure 3. Transcriptional inhibition of Gα12 by ERα

(A) Schematic drawing illustrating the principle of the Tet-On system used to ectopically express ERα in SK-Hep1 cells (*left*). qRT-PCR assays for *GNA12* in SK-Hep1 Tet-on system for ERα (Tet O-Erα) cells treated with 2 mg/μl Dox (or Veh) and continuously treated with 100 nM E2 for 24 h each (*right* , n =3 each, *p<0.05). Data were analyzed using the two-tailed Student's t-test.

(B) qRT-PCR assays for *GNA12* in SNU449 and HepG2 cells transfected with control and ERα O/E vector 1 μg for 24 h (*left*), and si ERα plasmid, 1 μg for 72 h (*right*) and 18S rRNA was used as internal control (n =3 each, *p<0.05 and **p<0.01). Data were analyzed using the two-tailed Student's t-test.

(C) qRT-PCR assays for *GNA12* in SNU 387 cells treated with 100 nM E2 in a time-dependent manner for 24 h (n =3 each). 18S rRNA was used as internal control (*p<0.05 and ***p<0.001). Data were analyzed using the ANOVA.

(D) ERE binding to *GNA12* promoter. ChIP assays were done on the lysates of SK-Hep1 Tet O-ERα cells treated with 2 mg/μl Dox for 24 h and 100 nM E2 for 24 h (*left*). DNA-protein complexes were precipitated with anti-ERα antibody and subjected to PCR amplification using the flanking primers for the ERE binding. IgG immunoprecipitation represents negative control and their quantifications (*right*) (n =3 each, *p<0.05 and ***p<0.001). Data were analyzed using the two-tailed Student's t-test.

(E) Luciferase assay structure is shown on the *top* and the relative luciferase activity measured on the *bottom* (n =3 each, **p<0.01). Data were analyzed using the two-tailed Student's t-test.

(F) Confocal images of Gα12 (green) and ERα (red), and Hoechst 33342 (blue) immunostaining in SK-Hep1 Tet O-ERα cells with 2 mg/μl Dox (or Veh) and 100 nM E2 treated for 24 h each (n =3 each, 4-5 replicates/group for each experiment; *p<0.05 and ***p<0.001). Data were analyzed using the two-tailed Student's t-test.

Figure 4. ERα regulation of EMT biomarkers via Gα12

(A) Immunoblottings for Gα12 and EMT markers using SK-Hep1 Tet O-ERα cells, treated with 2 mg/μl Dox and continuously treated with 100 nM E2 for nuclearization of ERα for 24 h each, as well as their quantifications (*right*) (n =3 each, *p<0.05). Data were analyzed using the two-tailed Student's t-test.

(B) Immunoblottings for Gα12 and EMT markers performed using SK-Hep1 Tet O-ERα cells transfected with Gα12 O/E plasmid (1 μg) or pCMV (Mock) (1 μg), treated with 2 mg/μl Dox and continuously treated with 100 nM E2 for nuclearization of ERα for 24 h each, as well as their quantifications (*right*) (n =3 each, *p< 0.05). Data were analyzed using the ANOVA.

(C) Immunoblottings for Gα12 and EMT markers performed using SNU449 cells transiently transfected with ERα or pcDNA (WT) (*left*), or SNU449 cells stably transfected with ERα O/E plasmid (1 μg) or Mock (*right*) for 24 h and continuously treated with 100 nM E2 for nuclearization of ERα for 24 h (repeated experiments).

16

(D) Immunoblottings for Gα12 and EMT markers in HepG2 cells transfected with si ERα or control for 72 h (*left*) and their quantifications (*right*) (n =3 each, *p< 0.05). Data were analyzed using the two-tailed Student's t-test.

(E) Immunoblotting for Gα12 and EMT markers in SNU387 cells (female HCC cell line) treated with 100 nM E2 for the indicated times (repeated experiments).

(F) Immunoblottings for Gα12 and EMT markers in SNU387 cells treated with E2 with or without ICI 182780, followed by 100 nM E2 treatment for 24 h and 1 mM ICI 182780 for 1 h before E2 treatment (repeated experiments).

(G) Immunoblottings for ERα, Gα12, and EMT markers in HCC-derived cell lines (repeated experiments).

Figure 5. miR-141 and -200a as inhibitors of PTP4A1 downregulation of ERα-Gα12 axis

(A) Venn diagram of miR-141 and -200a expression among the upregulated and downregulated miRNAs induced by 100 nM E2 treatment and Gα12QL. Gα12QL is an activated oncogenic mutant of Gα12. Notably, 42 miRNAs are up-regulated in the first set of estrogen-treated SNU387 cells; 104 miRNAs are up-regulated in the second set of estrogen-treated zebrafish; 138 miRNAs are down-regulated in the Gα12QL-Huh7 cells.

(B) qRT-PCR assays for ERα effects on miR-141 and -200a. miR-141 and -200a miRNA levels are increased by stable ERα overexpression on SNU449 cells (*left*). These cells were treated with 100 nM E2 for the nuclearization of ERα for 24 h. Decreased levels of miR-141 and -200a miRNA levels are observed by following knockdown of ERα in HepG2 cells for 72 h (*right*). U6 small nuclear RNA was used as a normalizing reference for miRNA (n =3 each, *p< 0.05, **p<0.01, and ***p<0.001). Data were analyzed using the two-tailed Student's t-test.

(C) qRT-PCR assays for estrogen effect on miR-141 and -200a. Increase in miR-141 and -200a miRNA levels following treatment with 100 nM E2 at times indicated using SNU387 cells (n =3 each, *p< 0.05 and **p<0.01). Data were analyzed using the ANOVA.

(D) qRT-PCR assays for exploring Gα12 effects on miR-141 and -200a. SNU449 cells were transfected with control siRNA (siCON) or siRNA directed against Gα12 (si Gα12). Transfection was done for 48 h (n =3 each, *p< 0.05). Data were analyzed using the two-tailed Student's t-test.

(E) qRT-PCR assays for showing miR-141 and -200a in control expression and SK-Hep1 Tet O-ERα cells with pCMV and Gα12 overexpression transfection for 24 h, followed by 2 mg/μl Dox and 100 nM E2 treatment for 24 h each (n =3 each, *p< 0.05 and **p<0.01). Data were analyzed using the ANOVA.

(F) An integrative network of putative or validated targets of miR-141 and -200a. Five hundred miR-targetable transcripts were analyzed using DAVID GO. From the significant pathways, biological process: regulation in cell migration was used to determine possible EMT regulators. Among the nine transcripts in the regulation in cell migration list, STRING analysis was used to distinguish the unknown yet important molecules to resolve EMT in HCC. Here, nodes represent genes/proteins, whereas edges represent interactions. Specifically, red nodes represent up-regulation in HCC; purples represent down-regulation in HCC; greens represent unknown in HCC; yellow circles represent involvement in migration; black circles represent predicted miR-141 and -200a binding targets.

(G) Prediction of miR-141 and -200a binding to the 3'-UTR of human PTP4A1 mRNA (*left*). The effect of miR-141 and -200a mimic and ASO treatment on PTP4A1 expression. Immunoblottings for PTP4A1 were done using SNU449 and HepG2 cells transfected with miR-141 and -200a mimic, ASO, or the respective control for 48 h (*right*, n =3 each, *p<0.05). Data were analyzed using the ANOVA.

(H) Immunoblottings for the effect of ERα on PTP4A1 expression. PTP4A1 was measured on SK-Hep1 Tet O-ERα cells treated with 2 mg/μl Dox for 24 h and continuously treated with 100 nM E2 for 24 h (*left*). PTP4A1 was measured on HepG2 cells with siERα transfected for 72 h (*right*, repeated experiments).

(I) Immunoblottings for the effect of Gα12 overexpression transfection on PTP4A1 with ERα modulation treated with 2 mg/µl Dox for 24 h and continuously treated with 100 nM E2 for 24 h (repeated experiments).

(J) Immunoblottings for the effect of PTP4A1 modulation with indicated PTP4A1 O/E or siPTP4A1 on EMT markers. PTP4A1 O/E vector (1 µg) was transfected on HepG2 cells for 48 h, and PTP4A1 was silenced on SNU449 cells for 72 h (repeated experiments).

Figure 6. Inhibition of amoeboid movement by ERα through Gα12

(A) Schematic drawing of cancer cells gaining invasiveness through phenotypic changes using matrix metallopeptidases (MMPs) or amoeboid transition.

(B) GSEA of HCC GEO data (GSE9843; Chiang DY, *et al.* , 2008) depicting pathway signatures of MAT positively correlated with male (versus female) HCC patients (n =27 females, and 53 males) (*left* , NES =1.91, FDR <0.25; and *right* , NES =1.57, FDR <0.25).

(C) 3-dimensional imaging of SK-Hep1 Tet O-ERα cells treated with 2 mg/µl Dox (or Veh) for 24 h, and continuously treated with 100 nM E2 for 24 h in a collagen I matrix (8~10 mg/ml) (*left*). Prior to imaging using time-lapse microscopy with controlled CO_2 (5%) and temperature (37°C) for 24 h or indicated times. The representative end point images are shown. Using ImageJ software embedded program ADAPT, blebbing and its velocity were measured throughout the time-lapse imaging for 24 h (*right* , n =3 each, *p<0.05 and ***p<0.001). Data were analyzed using the two-tailed Student's t-test.

(D) Representative confocal images of p-MLC (green), Gα12 (red) and Hoechst (blue) staining (n =3 each, *p<0.05 and **p<0.01). Data were analyzed using the two-tailed Student's t-test.

(E) Immunoblottings showing p-MLC expression in ERα overexpression SK-Hep1 cells with Tet-On ERα system for elucidating the effect of ERα on amoeboid movements (*left*). Immunoblotting showing p-MLC expression in ERα knockdown HepG2 cells for 72 h (*right*).

(F) Immunoblotting for the expression of p-MLC by modulating ERα and Gα12. (n =3 each, *p<0.05, **p<0.01, ***p<0.001). Data were analyzed using the ANOVA.

Figure 7. Changes of identified biomarkers under the control of ERα in animal dataset publicly available and human HCC samples

(A) Pearson correlation analyses for the relationships among *ESR1, GNA12* and *PTP4A1* in mouse xenograft GEO dataset (GSE94016, Yang B., *et al.* , 2018) (n =5 animals, 5 replicates). Gene expression was measured at five different time points as metastasis occurs. HCCLM3-REP mouse model was used and pulmonary metastasis was observed. Correlations were assessed using Pearson correlation analysis (r). Each point represents five samples at five different metastasis points.

(B) Immunoblottings for PTP4A1 and p-MLC. Protein levels were measured in 59 pairs of primary tumorous HCCs (T) and non-tumorous (N) specimens (*p< 0.05 and **p<0.01). Data were analyzed using the two-tailed Student's t-test.

(C) IHC for PTP4A1 and p-MLC (×200) (n =3 each, 4-5 replicates/group for each experiment, Scale bar, 100 µm) (*p< 0.05 and **p<0.01). Data were analyzed using the two-tailed Student's t-test.

(D) qRT-PCR assays to show gender disparity in the expression of newly found miR-141 and -200a (*left*). The ratio of T/N is lowly expressed in miR-141 and -200a in male (versus female) HCC patient samples. Data were analyzed using the Pearson correlation analysis. Symbols represent individual samples. qRT-PCR assays to explore the relationship of newly found miR-141 and -200a. Significantly positive correlations are observed between *ESR1* and miR-141 and -200a in the HCC samples (*right* , n =59, *p< 0.05 and **p<0.01). Data were analyzed using the two-tailed Student's t-test.

(E) Quantification of Gα12, PTP4A1, and p-MLC protein expression by sex. Higher expression of Gα12, PTP4A1, and p-MLC is observed in male (M) (versus female (F)) HCC patients without microvascular

invasion (n =40, 27 males, and 13 females, **p<0.01). Data were analyzed using the two-tailed Student's t-test. Outliers were removed with a range > 1.5 interquartile range.

(F) The schematic drawing the role of ERα-Gα12 in HCC progression through regulation of miR-141/-200a/PTP4Al and amoeboid movement.

Figure 1

Hosted file

figure 2.pdf available at https://authorea.com/users/378507/articles/494981-estrogen-receptor-alpha-inhibits-mesenchymal-and-amoeboidal-movement-of-liver-cancer-cell-via-g-protein-subunit-alpha-12

A)

B)

SK-Hep1 Tet O-ERα
E2 (100 nM)

SNU449

HepG2

C)

SNU387

D)

Putative ERE

Chr7 -1.5kb ——○—○—|+1|—→ GNA12
          2 1

Homo sapiens ERE sequences

Site #1 5'-TCAAGTGATCCTCCCACCTC-3'
Site #2 5'-CAAGGTTGTCAGGGAGTTGG-3'

Sk-Hep1
Tet O-ERα

Site #1   Site #2

E)

HEK293A
Gα12-Luci

Gα12-Luci —[Luc]—○——○—
                2   1

F)

Sk-Hep1
Tet O-ERα –E2 (100 nM)

	Gα12	ERα	Hoechst	Merge
Veh n=5				
Dox (2 mg/μl) n=3				

Figure 3

Figure 4

A)

Increased miRNAs by E2
F-Y Huang et al., Oncotarget, 2015
(n=40)

* Decreased miRNAs
in 12QL/Con

Y Yang et al.,
Oncotarget, 2015
(n=136)

25   10   113

miR-141
miR-122

15   13

74

Increased miRNAs by E2
(n=89)
A Cohen et al., zebrafish, 2014

B)

SNU449

miR-141   miR-200a

□ Mock
■ ERα O/E

*   **

E2 (100 nM)

HepG2

miR-141   miR-200a

□ si Con
■ si ERα

***   *

C)

SNU387

miR-141   miR-200a

**   *

E2 (100 nM)   0 12 24 (h)

D)

SNU449

miR-141   miR-200a

□ siCon
■ si Gα12

*   *

E)

Sk-Hep1 Tet O-ERα
E2 (100 nM)

miR-141   miR-200a

□ Mock
■ Gα12 O/E

**   **

* *   ** **

− + − +   − + − + Dox (2 mg/µl)

F)

GO: **Regulation of cell migration**

GRB2
INSR   GAB1   PIK3R1   GNA13
IRS2   AKT1   TAC1
PTEN   PTPN11
PTP4A1   DLC1

G)

PTP4A1 3' UTR 5' ...GAGAAAUAAUUUUGUCAGUGUUC...
hsa-miR-141-3p 3' GGUAGAAAUGGUCUGUCACAAU
/200a-3p

SNU449   HepG2

□ WT
■ miR-141
■ miR-200a

* *   * *

mimic   ASO

SNU449   HepG2

PTP4A1
β-actin

PTP4A1
β-actin

15
40
(kDa)

* *   *

H)

Sk-Hep1
Tet O-ERα −E2 (100 nM)   HepG2

PTP4A1
1.00 0.32   1.00 1.22

ERα
1.00 21.6   1.00 0.09

β-actin

15
55
40
(kDa)

I)

Sk-Hep1
Tet O-ERα −E2 (100 nM)

Mock   Gα12 O/E

PTP4A1
1.00 0.25 1.87 4.86

Gα12

ERα

β-actin

− + − + Dox (2 mg/µl)

15
40
55
40
(kDa)

J)

HepG2   SNU449

Vimentin
1.00 2.59   1.00 0.41

E-cadherin
1.00 0.30   1.00 1.42

PTP4A1
1.00 2.33   1.00 0.02

β-actin

55
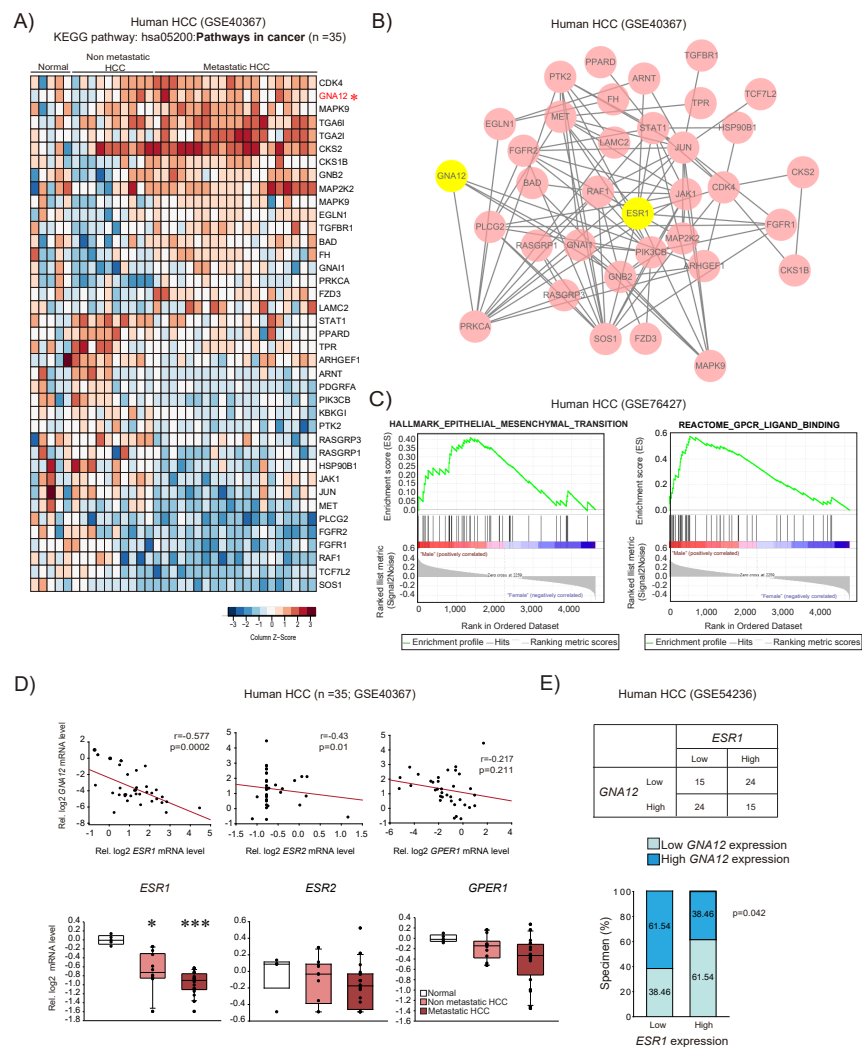100
15
40
(kDa)

Figure 5

22

Figure 6

Hosted file

figure 7.pdf available at https://authorea.com/users/378507/articles/494981-estrogen-receptor-alpha-inhibits-mesenchymal-and-amoeboidal-movement-of-live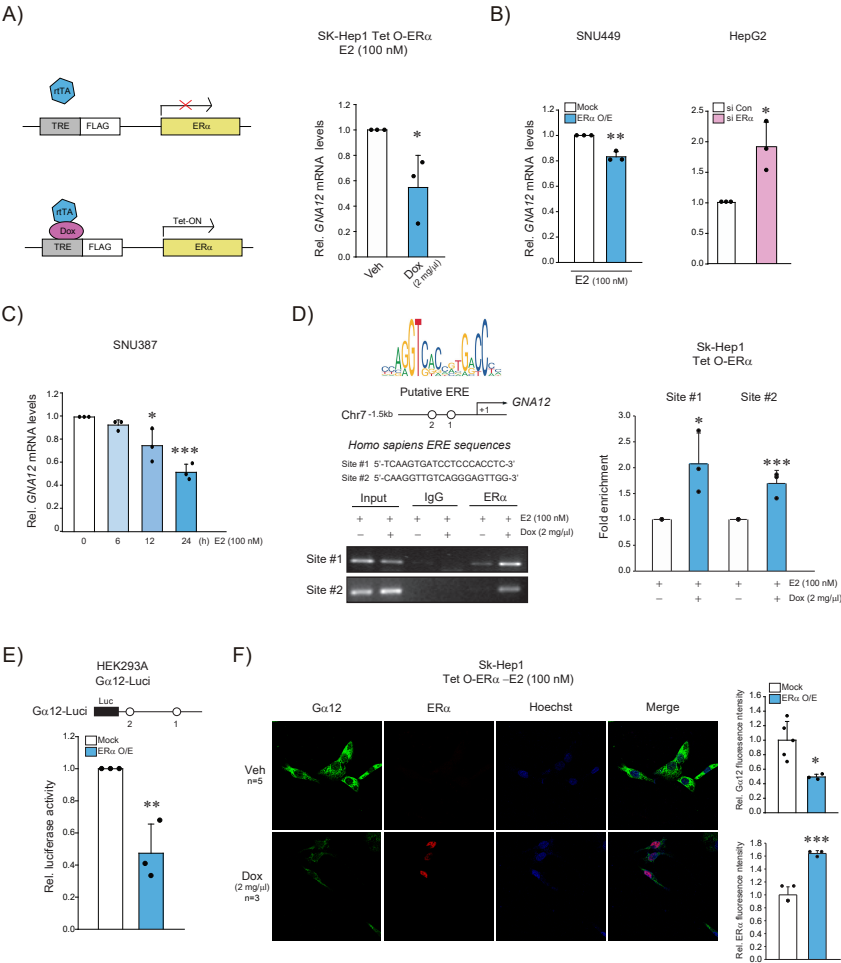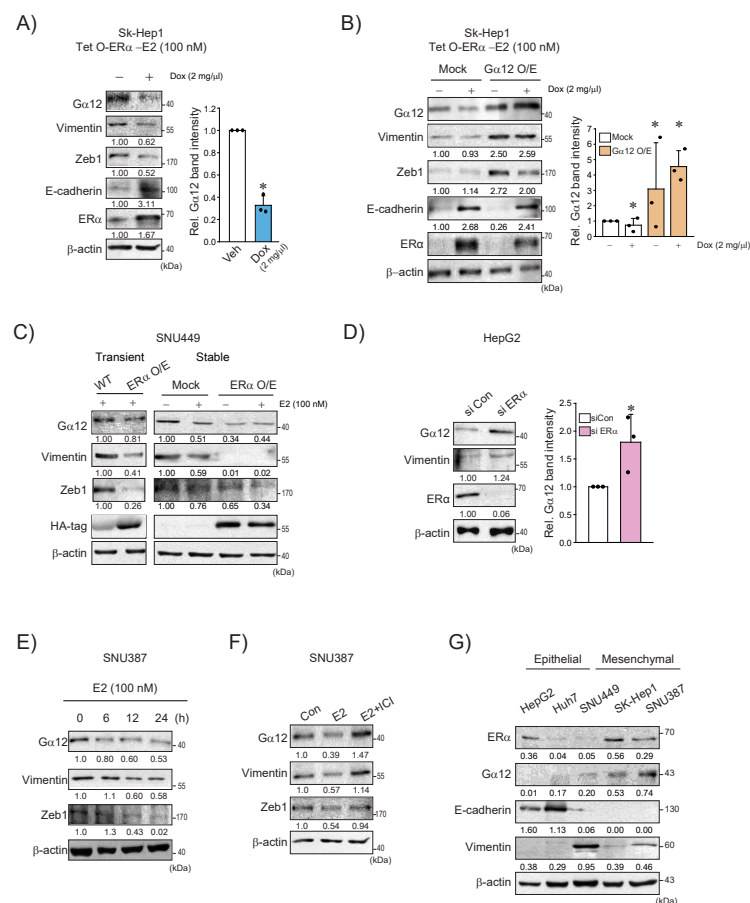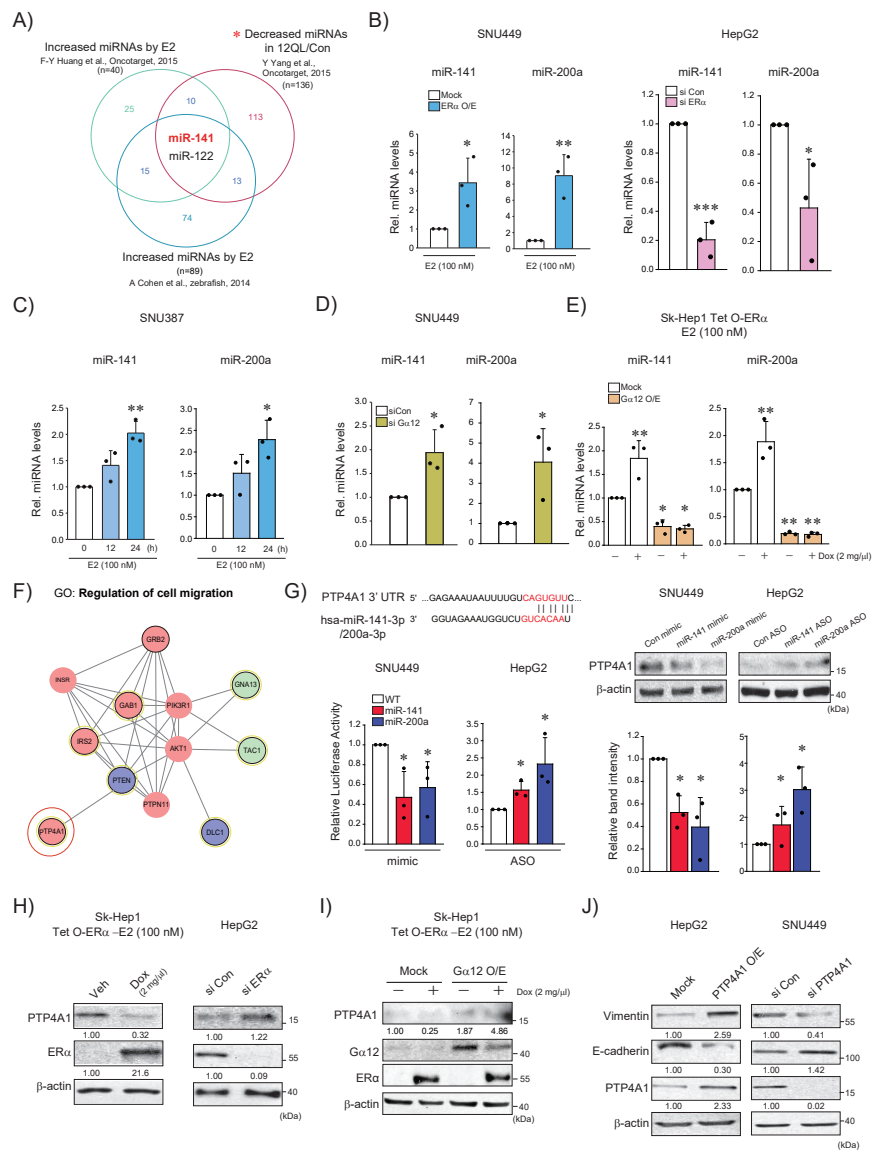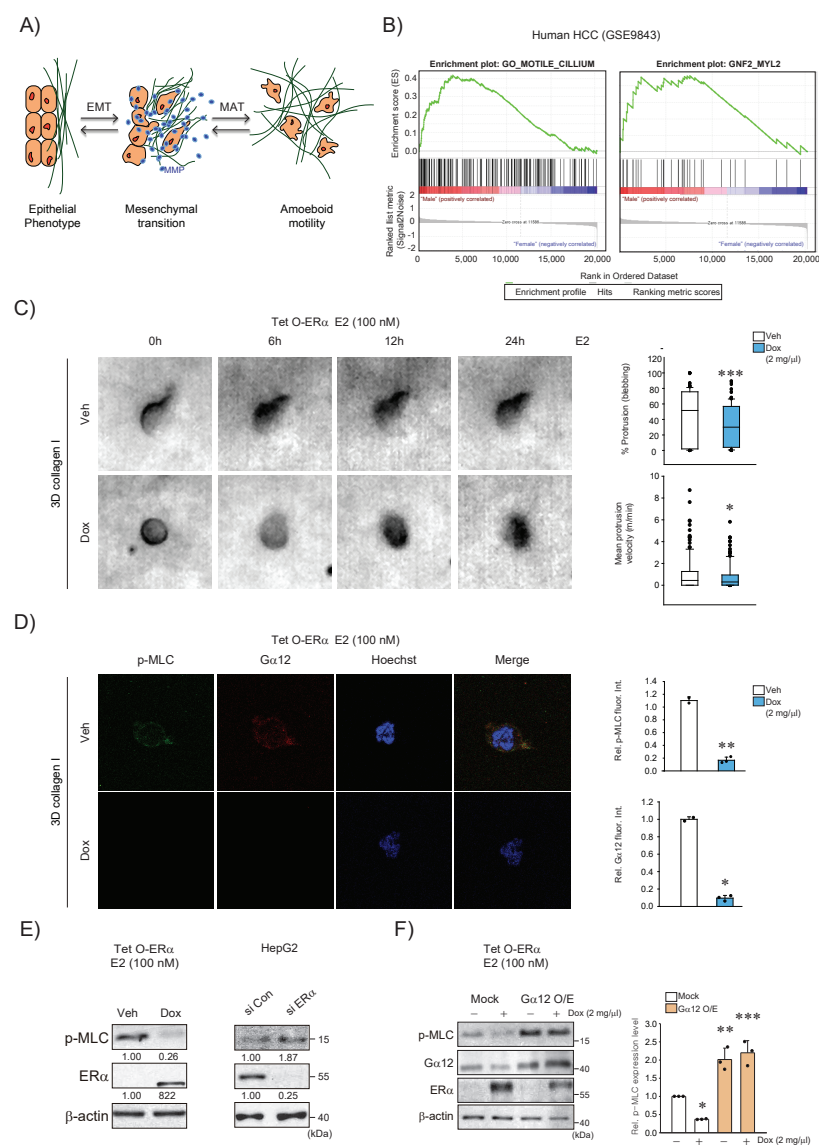r-cancer-cell-via-g-protein-subunit-alpha-12